RESEARCH ARTICLE

A Methodology Proposal for Conducting a Macro-PK Test on Light Spinning Objects, in a Non-Confined Environment

ERIC DULLIN

ericdullin@gmail.com

DAVID JAMET

Psychophysics Anomalies and Cognitive Dissonance Laboratory (LAPDC), Poitiers, France

Abstract—For more than a century, there has been much debate around the use of telekinesis–psychokinesis (TK)[1] to explain the rotating movement of light objects on an upright standing needle in the proximity of a hand. Thermally induced aerodynamic effects have been considered as likely physical explanation factors. Despite this controversy, many people still upload videos claiming the phenomenon on the Internet. Most of the scientific studies performed were focused on whether or not the effects could be observed if some physical constraints were added, in order to avoid the aerodynamics factor, or if the same results could be reproduced using some thermic or/and aerodynamic artefacts instead of a human presence. The first approach runs the risk of inhibiting a phenomenon about which little is known. The second has not yet shown clear reproducible experiences, which produce the same results as with a human presence, except in very specific situations. Our objective is to be able to detect and study psychokinesis in confined and non-confined environments with scientific measurement tools. Our hypothesis is that there could be a way to separate psychokinetic effects from aerodynamic effects, even in a non-confined environment, thereby avoiding the drawbacks of the first approach. This technique of approaching anomalous perturbations could be described as partial physical isolation of the target system, with a measurement system ensuring control of the remaining known effects. It can be related to two other techniques previously described (May, Utts, & Spottiswoode 1995: Introduction). From the beginning, the LAPDC (Psychophysics Anomalies and Cognitive Dissonance Laboratory) has been fostering a PKers (subjects practicing psychokinesis) volunteer team in order to do the experiments. From 2012 to 2016, we were developing specific scientific methods in order to study the psychokinesis effect on a spinning mobile with or without confinement. More specifically, we developed a protocol starting with particle

image velocimetry (PIV) in order to measure the air-flow speeds around the mobile. Further research has driven us to create a set of processes using MATLAB, which we named Scan-Flow-Mobile. It has enabled us to construct one global model, integrating air flow movements and mobile movements, and to scrutinize it. Using this, we were able to compare different experiments. We conducted a thorough analysis of the interaction between the mobile and the air flows, and studied the cause-and-effect relationships between their movements. A review of the "spinning mobiles" literature of the last century, either with a psychokinetic hypothesis or an aerodynamic/thermic explanation, has been done. We also studied other potential causes of motion such as electrostatic forces, magnetism, vibrations, and the impact of radiation. Then, as a pilot study, we conducted eight experiments in non-confined environments, with three setup categories: one where the mobile motion was driven by generated air flows (A), one in which a motor drove the mobile (M), and the last one where a PKer drove the mobile (PK). The ratio (mobile speed / mobile periphery airflow speed) was used as a way to compare experiences between experiments and categories. In this paper we focus only on the methodological approach and so on the categories A and M. With regard to this ratio, the category M experiments stayed above or equal to 2, while category A was below or equal to 0.5. This clearly separated purely aerodynamic effects (A) from the motor-driven effect (M). The methodology could be a good candidate to conduct a macro-PK test in a non-confined environment with the capability to eliminate or not the aerodynamic effect as the explanation. A potential bias and errors analysis is presented, which takes into account the difference between air-flow and smoke-particle velocity, the mean speed evaluation for the air flows and the mobile. Indeed, we evaluated the potential error on the ratio air-flow speed/mobile speed as approximately ±8.9%, which is marginal compared with the ratios differences between categories A and M. The methodology also presents some features that help to detect tricks that could be tried by some misbehaving PKers (e.g., mouth air blowing, hand movements, etc.). We will continue to look to improve documentation of the total measurement process, in order to give other laboratories the potential to test it in their experiments.

Introduction

Is Psychokinesis on Small Objects Widespread or Non-Existent?

Nowadays, we can find on the Internet many videos with different kinds of "psi wheels" claiming the evidence of a psychokinetic effect.[2] Many Internet forums[3] are skeptical about these claims, however, and announce that all of these videos are fakes, or at least show some classical aerodynamic effect induced by the heat of the hand.

Where does the truth lie? Are there scientific studies available on the subject?

It is well-known that it is not possible to prove any null hypothesis. The null hypothesis is generally assumed to be true until evidence indicates otherwise. Here, the null hypothesis is: "There is no relationship between a 'psi wheel' movement and a human presence, except through known physical forces."

A Long Story from Mesmerism and Magnetic Fluid to Vital Energy

By the end of the 18th century, Franz-Anton Mesmer had developed his animal magnetism theory, proposing that all living beings were emanating some kind of "fluid" that was capable of healing others and inducing trances. This theory had great influence until the beginning of the 20th century, and several individuals tried to develop a mechanism to measure this ostensible "magnetic fluid" or "bio fluid."

The French physician Hypolyte Baraduc (1893) used an instrument he called a biometer, which consisted of a glass jar inside of which was a needle suspended by a thread. The needle rotated on top of a circular surface with numbers, which allowed Baraduc to obtain readings corresponding to the movement of the needle. When people put their hands near the instrument, the right hand effected an attraction on the needle whereas the left hand repelled it. These movements, described by Baraduc as "tangible and recordable expressions of a superior Force," were considered to be evidence for the existence of a vital body in human beings (Alvarado 2006).

Another French parapsychologist, Paul Joire, devised an instrument call a sthenometer (Figure I1). This, he claimed, could detect the "nervous force" emitted by the body, and he published several papers on the topic.

Le Comte de Tromelin, a French physician and inventor, proposed a motor driven by "human fluid," which was easy to build (Tromelin 1907). He produced several publications such as the one in *Le Monde Psychique* (Tromelin 1912) from whom the pictures below are extracted (Figure I2). These motors were mainly composed of a light object attached to a needle which sat on top of a metallic support (or at least a smooth surface so that the needle could spin.

People then performed more tests and research on these kinds of mobiles. Pierre Archat built some testing equipment using an approach to prevent or balance the aerodynamic thermally induced forces, in order to see if some remaining effects persisted (Archat 1908). His objective was to study whether any person could generate a motor action on a living being or on an object in their proximity. Figure I3 shows one of the setups he used. Here, the object O is placed on a torsion mobile B, itself inside a bell jar C. The subject approaches it with their hand, M, close to C without touching it.

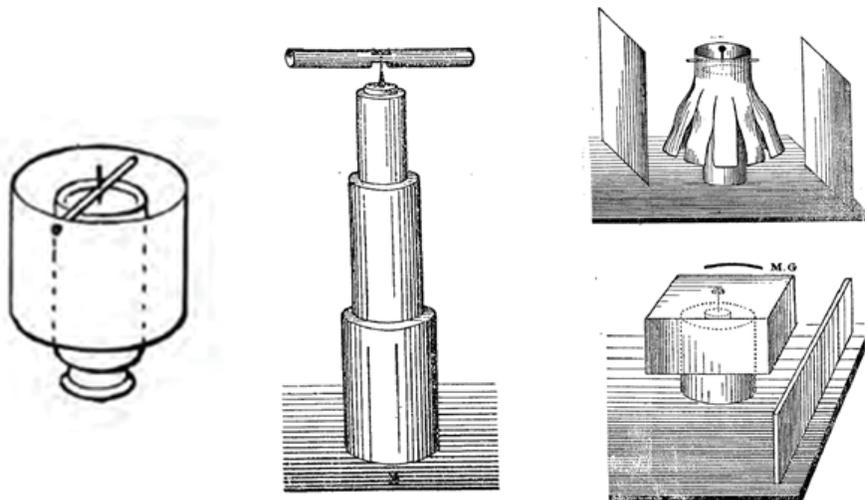**Figure I1. In** *Le Petit Parisien* **newspaper, December 26, 1908.**

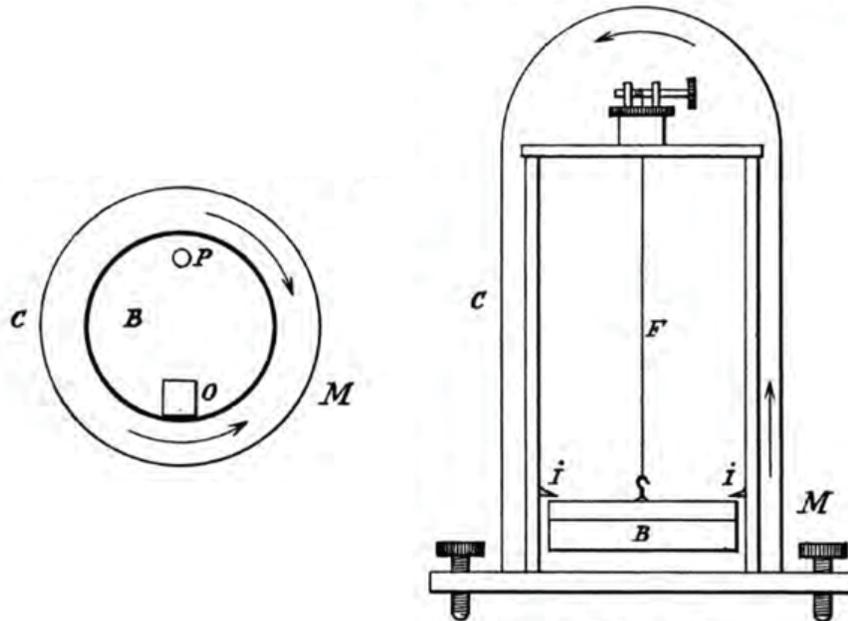**Figure I2. Examples of Tromelin's motors (Tromelin 1912).**

Figure I3. Archat "telekinesis" testing machine (Archat 1908).

Here is an extract of his translated conclusion (Archat 1908):

It is right that this apparatus is less sensitive than the first one because the weight of B is ten times the one with only a needle. But no deviation, even small, has been observed, even with the use of a 5–6 times magnifying glass. My research stopped there. If the result is negative, I think it's not a good approach to conclude that the force I was looking for didn't exist, but we need to study it by other means than the one I used. It seems that we could deduce from these experiences that this force is not emitted in a continuous way and with an appreciable strength by the human organism. Perhaps it exists in a latent state in the organism and manifests itself only in certain conditions. Indeed, it is possible that the result could have been different with a medium with physical effect: This experiment has not been done.

At the same Congress, René Warcollier outlined his analysis and criticisms of Tromelin's book (Warcollier 1908). He proposed some explanations as described below (Figure I4): Human body heat creates a rising airstream. This upward airflow draws air above the table, and induces an airstream in the direction of the subject. The hand, forming an obstacle to this airstream on the right, creates a dissymmetry in the aerodynamic forces
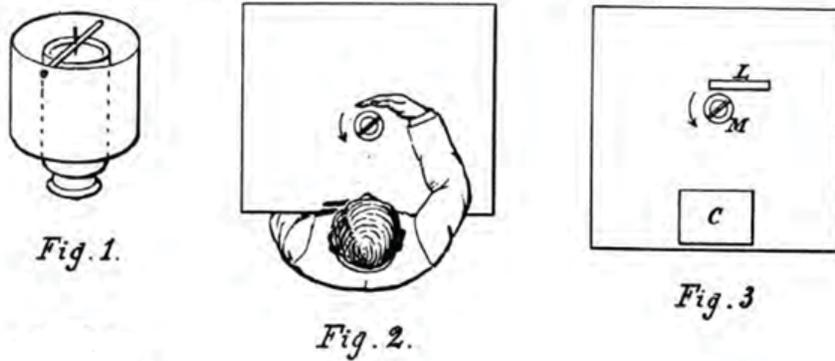
Figure I4. Warcollier's explanation of Tromelin's motor movement (Warcollier 1908).

around the mobile. This creates a resulting torque that spins the mobile. Figure 3 inside Figure I4 proposed a way to simulate the phenomenon without a human presence using a calorimeter as a heat source and a book as an obstacle.

In Russia, Yakov Perelman published the first release of his book in Russian *Physics for Entertainment* (Perelman 1913), translated later into many languages. In his book, on p. 117, he exposed "The mysterious twirl" with the picture in Figure I5. His explanation was:

> when you bring your hand up, the air near it, which is warmed by its proximity, rises, and, pressing against the piece of paper, causes it to spin. It revolves because it is slightly folded, thus performing the same role as a curled piece of paper suspended above a lamp.

Then he referenced Nechayev, who in 1816 wrote a communication to the Moscow Medical Society entitled "The Gyration of Light Bodies Caused by the Heat of the Hand" (we did not succeed in obtaining this communication). Using this reference, Perelman explained why the piece of paper always gyrates in one and the same direction—from the wrist toward the fingertips. It is because the fingertips are always colder than the palm of the hand; consequently, the palm gives rise to a stronger ascending air current than the fingertips do.

In France, Clément Martin did a further analysis of the Archat/Warcollier results using an apparatus on which people can apply the hand touching it at different positions (Martin 1926). With two glass containers V and V', it was able to simulate the temperature difference between the center of the

Fig. 82. Why does this piece of paper spin?
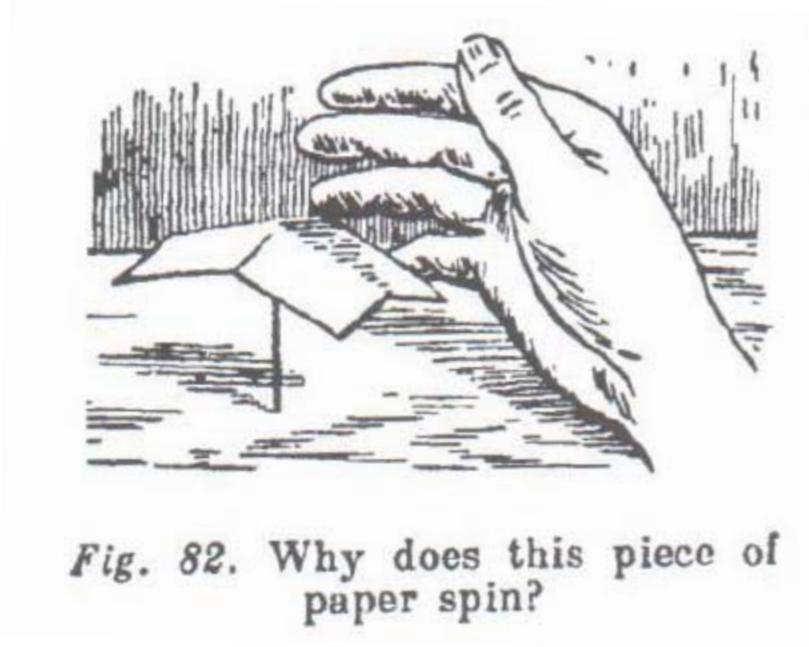
Figure I5. The mysterious twirl (Perelman 1913).

hand and the fingertips (Figure I6). His final statement was that no force other than an aerodynamic and thermic one has been demonstrated, and that in a confined environment serious consideration must to be given to the size of the "air column" (Martin 1926).

Tromelin's motor came back in another form with the work of the Czech physicist Julius Krmessky, who developed some mobiles with light objects which were very close to Tromelin's (Figure I7). He used them as "ideal research tools, since they are simple, inexpensive, and require no special training or psychic talent for their operation." Krmessky recommends isolation of the system from the motion of air and the effects of heat radiation by enclosing it in glass, metal, or other containers, with provision for inspection through a glass cover. Here are some of Krmessky comments about his results:

> Movement in such enclosed spaces are slow and hence not too spectacular, but are nevertheless convincing. The slow rate of the motion or the occasional immobility cannot be explained by the walls being impenetrable to outside impulses, because the device is able to detect the nearing of a hand, even through a thick layer of lumber, metal, water, etc. The cause lies somewhere else. (Krmessky 1975)
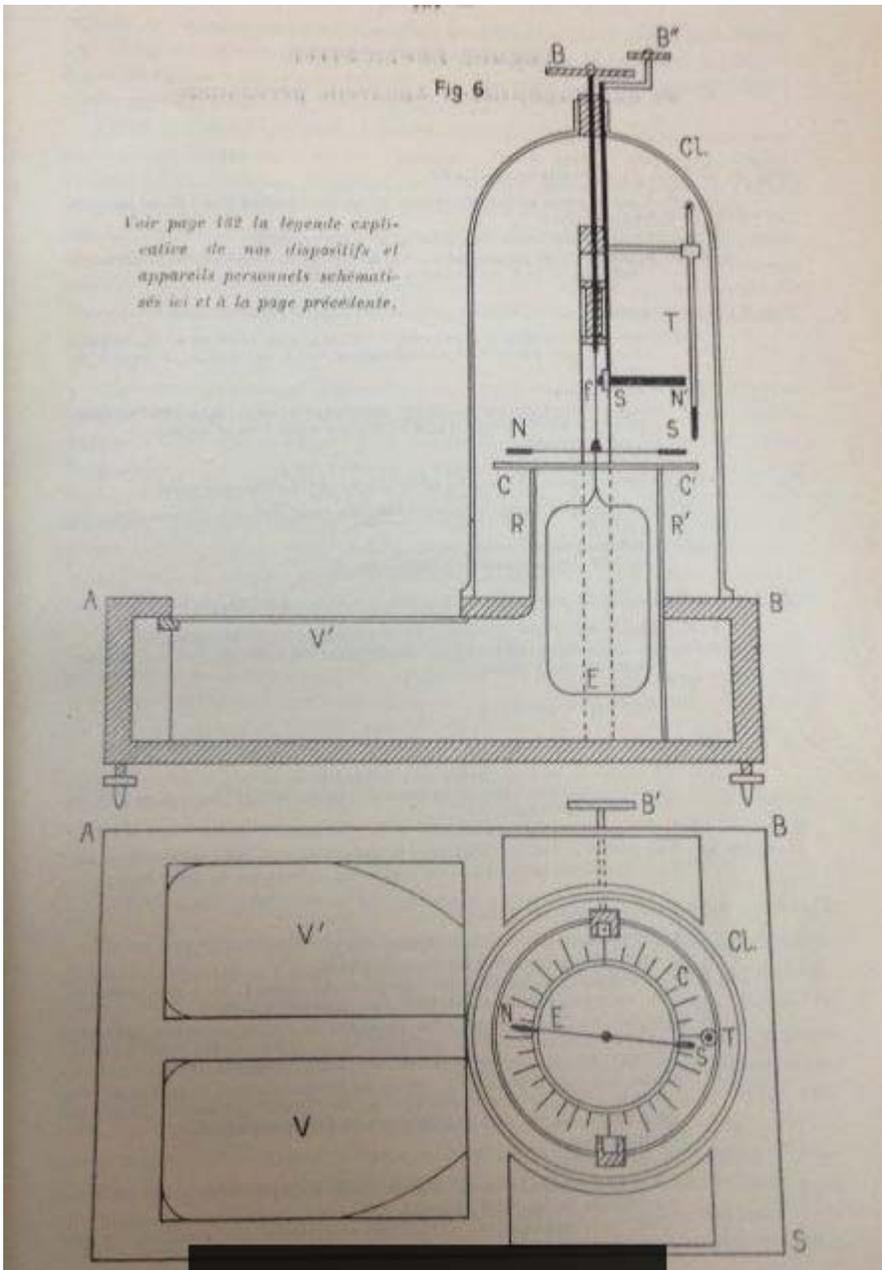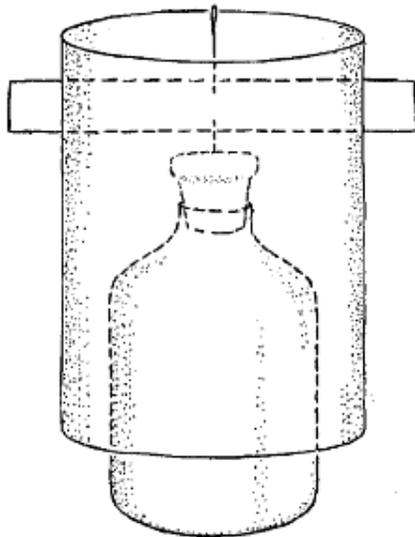
Figure I6. **Clement Martin's apparatus with the two containers V and V' (Martin 1926).**

Figure I7. Krmessky's pyschotronic rotor (Krmessky 1975).

Thanks to Edwin C. May and Loyd Auerbach (Auerbach 1996), we discovered the work of Martin Caidin in the USA. Following the publication of G. Harry Stine's book (Stine 1985), Martin Caidin conducted many experiments around the "Energy-Wheel" (an object, like a pyramid of paper, balanced on a pin) and wrote his journal of the experiment "The Merlin Effect," in which he advocated for a specific effect with hands close to the object (even inside a jar) but also from a distance (by using a mirror to look at the target or even through a TV Monitor or a camera). However, he pointed out the importance of the distance on the strength of the effect. He also reported being able to control in some cases in which direction the wheel should spin, to stop it, and to reverse the sense of rotation. He also observed a growing difficulty in increasing the weight of the target (he experienced a learning curve from a tenth of a gram to 450 g). He also mentioned the "use it or lose it" rule: If you do not practice for a while, you have to start from the beginning with a low weight and climb the ladder again with increasing weight targets.

Thanks to Professor Peter Mulacz (head of the parapsychology association in Austria), we discovered the work of Albert Hofmann (Hofmann 1919/1992). We did not succeed in getting a copy of the book (the title can be translated as "the mystery of the radiating hand"), but Professor Mulacz summarizes Hofmann's finding as:

Figure I8. The Egely wheel (Egely 2017).

    * with a hollow rubber hand filled with 37° C water ==> no effect
    * with a pulsation of the adjacent air ==> mobile starts rotating
    * his interpretation: It is the pulsation of the bloodstream in the hand
       (at the wrist, where the doctor feels the pulse) that is the cause of
       that air effect.

More recently, John Rudkin published an article focused on the Egely wheel. This instrument is a commercial product (Figure I8) which the manufacturer claims is able to measure life energy, chi, or vitality. The subject just has to look at the speed of the wheel when their hand is placed close to it (Egely 2017). It is a typical ¨psi wheel": a light plastic wheel of approximately 3.5 inches spinning on a pin. Rudkin's concluding statement on his study was "The behavior I have observed of the Egely wheel and similar spinners is explicable in terms of thermally induced aerodynamic effects" (Rudkin 2001).

Although it is not a spinning mobile on a needle, but rather a torsion pendulum with small effect, we could also mention:

— The work of J. N. Hansen and J. A. Lieberman on a torsion pendulum placed as a helmet above the subject's head to detect brain impact without contact (Hansen & Lieberman 2013).
— The research of Dr. Antonio Giuditta on the human bioenergy field, with a torsion pendulum placed at a distance of one meter from the subject (Giuditta 2014).

Finally we would like to mention the recent work of John G. Kruth, who led experimental sessions with an exceptional participant using an Egely

wheel (Kruth 2016). The Egely wheel was covered by a plastic container sealed with the support. The protocol eliminated other causes of movement. The participant was able to move the wheel at a distance of up to 12 inches. On average, a full rotation required three minutes. The participant required time (one day) to adapt herself to the laboratory's Egely wheel, even if she had her own Egely wheel.

TK–PK

In Varvoglis and Bancel (2015), psychokinesis (PK) is defined as follows: "PK is the putative ability of organisms to affect other systems—both animate and inanimate—without mediation of any known physical forces or energies." We agree with this neutral definition, in which the mind/human intention is not necessarily concerned. So, at the LAPDC we prefer to use the term telekinesis (TK) instead of PK. However, as the vast majority of parapsychological publications in English explicitly use the term PK, we use the term PK in this paper (and PKers for persons practicing psychokinesis).

Macro-PK or Micro-PK

As described in Watkins (2015), macro-PK is a term used to describe ostensible psychokinetic effects so strong or so dramatic as to require no use of statistics. It can also include levitation and teleportation. Even with small effects, we do not need to use statistics to study the phenomenon described above. Therefore, we are in the macro-PK space, also named macro anomalous perturbation (macro-AP) (May, Utts, & Spottiswoode 1995).

Our Objective: A Third Way to Study Anomalous Perturbations

For most of the previous research described above, the pros and cons of the existence of small psychokinetic effects, producible by non-exceptional subjects, are presented. They also describe, as presented by Jahn and Dunne (2011), that uncertainty using fewer constraints could be a prerequisite for seeing larger phenomena. Indeed, as we saw above, the effect seems to disappear or become very small when increasing constraints and confinement are applied (for example, Krmessky's low motor speed in the confined environment and the Egely wheel speed in Kruth's experiment).

Our objective is to study these small effects in more detail, with new scientific means and methods that do not require confinement, in order to identify whether aerodynamic forces could really explain all these mobile-spinning effects or not. In fact, our proposition is an extension of that by May, Utts, and Spottiswoode (1995:p.196) that two techniques have been

employed to study anomalous perturbations. These are:

1. complete physical isolation of the target system,
2. counterbalanced control and effort periods.

In this paper we try to show that there could be a third way: "partial physical isolation of the target system, with a measurement system ensuring control of the remaining known effect." The advantages are developed in the Methods section, in the subsection entitled ***Looking for Clear Anomalies versus Significant Deviation from Null Hypothesis on a Set of Calibrated Experiences***.

Methods

Our approach at LAPDC is to look for subjects with some potential psychokinetic capabilities (PKers), thus able to produce rather regularly some small effects (the word "rather" is important here as the effects are not systematically produced). The difficulty when working with small effects is that a small effect implies a small signal, making it harder to detect and separate from the environmental noise. This is the well-known problem of the signal-to-noise ratio (SNR).

As explained in the ***Our Objective*** section above, the focus of this paper is on the analysis of aerodynamic forces. Other potential factors that can move a light mobile have been discarded, including magnetic and electrostatic forces, vibration, and radiation.

- Magnetic forces were eliminated by choosing a mobile made out of plastic.
- We performed tests with electrostatic forces (Figure M0e) but were unable to drive the mobile more than a half turn (the mobile swung between two positions and then stabilized itself).
- We obtained the same results with forces induced by mechanical vibrations. Vibrations from 10 Hz to 20,000 Hz were generated with a loudspeaker and measured using a smartphone accelerometer (Figure M0v). We never observed a movement larger than a half turn.
- For the effect of radiation, its impact is to be combined with the aerodynamic thermally induced effect analysis, radiation pressure being marginal.

For further details on the tests above you can consult LAPDC's website on the physical approach: https://sites.google.com/site/lapdctk1/LAPDC_Protocole_1a/hypotheses-classiques.

Figure M0e. Electrostatic test with a generator.

Figure (M0v). Vibration test using an accelerometer.

We developed some specific experiments to separate psychokinetic effects (if existent) from aerodynamic and thermally induced effects. The method does not require that the mobile be confined. This enlarges the ef-

fects we can observe (in particular, the observed speeds are greater in a non-confined environment). We attempt to model the details of the physics involved, to gain a deep understanding of the results and to be able to investigate their potential causes.

Experiments Explained in This Paper

In this paper we will focus on one specific type of experiment using the same kind of spinning object. The aim is to compare the speeds of the air flows surrounding the object to the speed of the object itself. The complete approach for each experiment is detailed below.

Three different kinds of experiments have been compared:

- experiments producing mobile movement with an airstream (called A experiments),
- experiments in which the mobile spin is produced by a motor-drive (called M experiments),
- experiments which produced movement when a PKer put their hand close to the mobile (called PK experiments)

In this paper focused on the methodology, only A and M experiments will be presented.

The A experiments will show what kind of aerodynamic effect is able to spin the mobile. M experiments will show what happens to the air-flow speeds around the mobile when the mobile is spun by a small electric engine (and not aerodynamic effects). Besides serving as reference experiments against which the macro-PK test experiments (PK) could be compared, these A and M experiments were also a way to test and validate the measurement chain process.

To compare the experiments, the following ratio will be evaluated: mobile speed / mobile periphery air-flow speeds.

Indeed, as an energy transfer principle, if it is only aerodynamic effects that drive the mobile, then the air-flow speeds around the mobile have to be greater than the mobile speed, at least in some areas. So, if the value of the above ratio is smaller than 1, then the air-flow speeds on the mobile periphery are greater than the mobile speed, and we can infer that the air stream is able to drive the mobile. Therefore, aerodynamic forces are the probable cause for the mobile movement. If the value of the above ratio is larger than 1, the air-flow energy is insufficient to drive the mobile at this speed, and other explanations apart from aerodynamics forces must be found. Indeed, there is always some kind of energy waste in the transfer of energy between the air flows and the mobile, so a ratio equal or close to 1 is not sufficient.

Figure M1. Hemispherical mobile device used for the experiments.

Hemispherical Mobile Device (HM)

The first step was to choose a standard mobile device. A plastic dome (with a hemispherical shape), easily found in retail shops, was chosen (Figure M1). The shape and the smooth surface give little grip for the air flow to take hold. This dome is placed on top of a needle inserted in a plastic support or cork. The weight of the dome is 2.4 g and its diameter is 85 mm.

Air-Flow Speeds Measured by PIV

To analyze the impact of aerodynamic forces on the mobile, the first task is to be able to measure the air-flow speeds around the mobile. In this context, we work with low speeds (a few cm/s to 20 cm/s). Through collaboration with the Pprime laboratory of Poitiers University, the particle image velocimetry (PIV) technique was selected as the way to measure these speeds.

The principles of the PIV experiment we used are as follows (Figure M2):
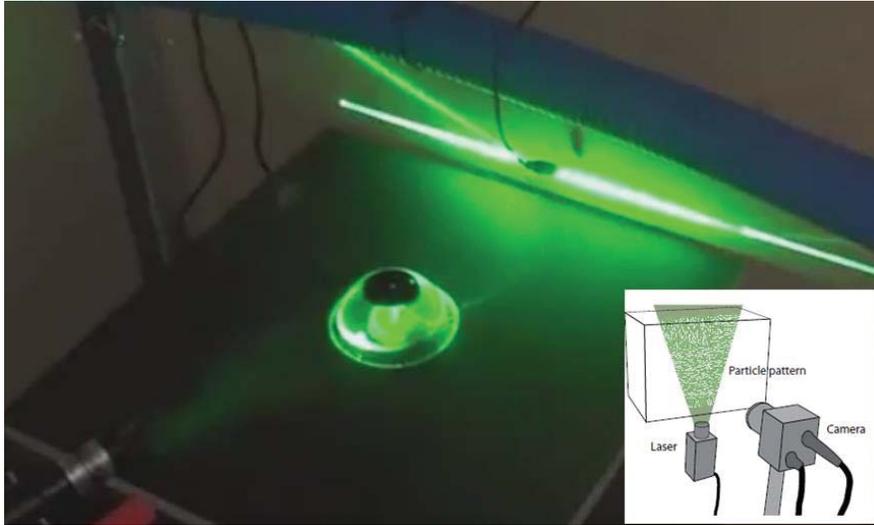
Figure M2. PIV test bench and principle.

— a laser beam illuminates a thin horizontal air slice just below the hemispheric mobile (HM) or at a specific height on the mobile,

— smoke is introduced (with a classic fog machine and some dispatcher pipes, sometimes helped by a small fan),

— the laser light diffuses on the smoke particles or/and smoke particle aggregates,

— a camera records the images (in our lab we use a 1080 x 720 definition sensor at a speed of 50 images/s),

— specific image processing software is used to deduce the speed of the smoke particles using their position change between two sequential images.

At LAPDC, we use PIV LAB, a MATLAB application developed by Thielicke and Stamhuis (2014). With this software we perform a pattern analysis using a fast Fourier transform (FFT) correlation algorithm, with multiple passes and deforming windows. Briefly, the software starts from the image pixels, compares two images, and tries to recognize identical patterns (particles aggregates or particles) in these two images (which may have rotated). Once some identical patterns have been identified, the software computes the pattern shift between the two images (Figure M3: ΔX, ΔY). By using the time elapsed between the two images (Δt), the software is able to calculate the pattern speed and direction (U,V).
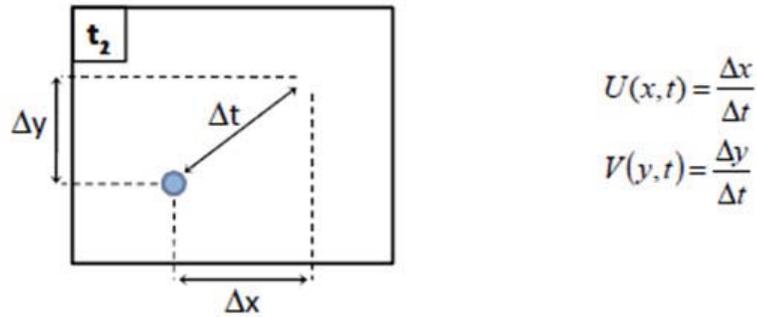
$$U(x,t) = \frac{\Delta x}{\Delta t}$$

$$V(y,t) = \frac{\Delta y}{\Delta t}$$

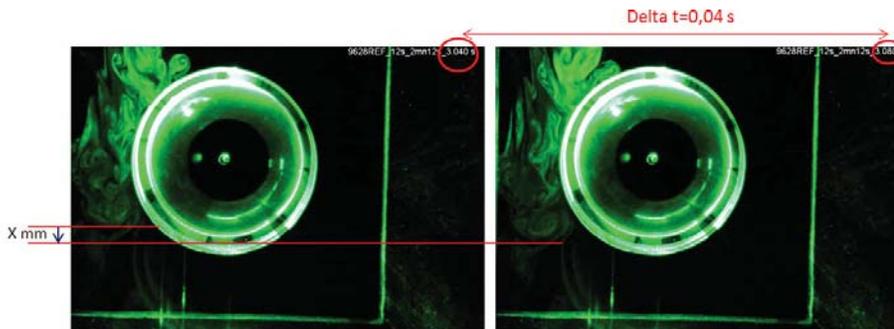**Figure M3. Speed measurement principle.**

Figure M4. Speed measurement principle used by PIV LAB.

To illustrate the process, we present (Figure M4) two sequential images separated by 40 ms ($\Delta t = 0.04$ s). The smoke cloud front moved X mm during this time, so the speed of the point situated at the front of the cloud is $X/0.04 = 25 * X$ mm/s. In this case there was a vertical shift only in the V direction.

Using the same process with all the identical patterns that could be detected, the software identifies the speed at many different points. It then calculates, by interpolation, a matrix representing the speed vectors field. Figure M5 gives a representation of the speed vectors field between these two images of the sequence. The narrow green and orange arrows represent the speed vectors at different points of the image. Orange arrows were obtained by interpolation when information was not sufficient for the system to compute the speed at certain points.

The software makes this process for image 1 and image 2, then image 2 and image 3, then 3 and 4, and so on. After that, it is possible to check some speeds at a specific time and a specific position or to ask for the mean speed vectors field on the total set of images, as shown in Figure M6.
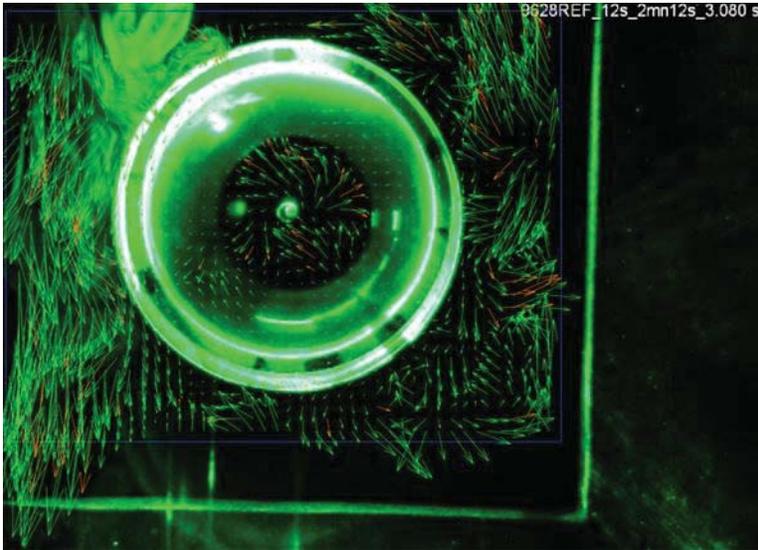
Figure M5. PIV results: speed vectors field between two sequential images.
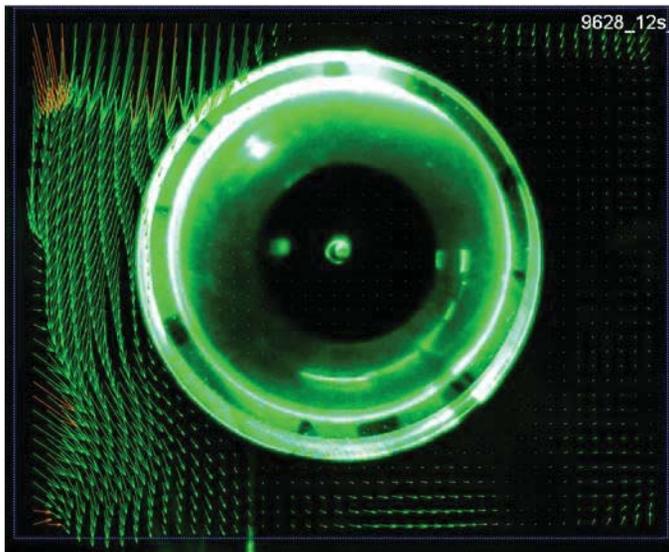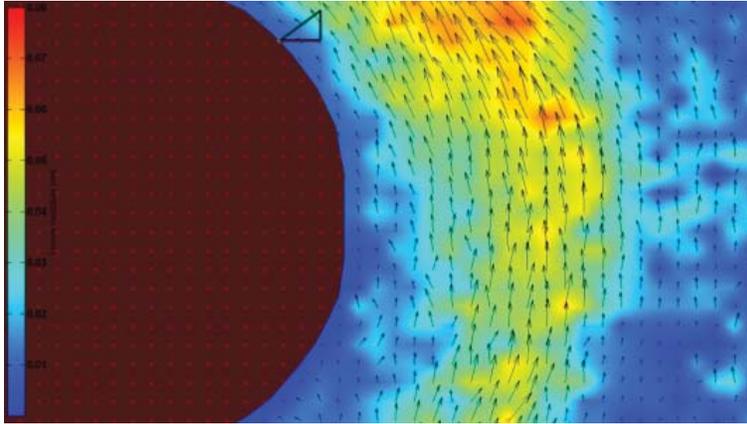

Figure M6. Vector-field representation of the mean air-flow speeds around the mobile.

**Figure M7.   Color representation of the air-flow speeds around the mobile.
                        Mobile is in red/brown. Other colors are associated with the
   range of air-flow speeds.**

Tools are available to study some parts of the air-flow movement in detail, or to show quickly, with color, the areas with a specific range of speeds (Figure M7).

Scan-Flow-Mobile Software

The preceding analyses are interesting to check air-flow speed at a specific time, in a specific area around the mobile, or the mean air-flow speed during a time interval in a specific area. However, in order to analyze the air-flows speed evolution with time around the mobile, compared with the mobile-speed evolution, further tools were necessary. So we developed a set of procedures using MATLAB, which we named Scan-Flow-Mobile (Figure M8). They enable us to model the complete experience (movement of air and the mobile) as a numerical object and zoom in on some parts of the process (in space and time) with different granularity levels. With this tool we can compare different experiments and perform a fine analysis of the interaction between air flows and the mobile, and identify cause-and-effect relationships.

The first step is to extract from the previous calculation (done with PIV LAB) the tangential speed on concentric circles around the mobile. Each circle is represented with 100 points that are equidistant from each other. The distance between each circle is 1.5–2 mm. In parallel, a calculation of the curve representing the mobile speed evolution is performed using the software Tracker. The starting point is the same video used by PIV LAB to
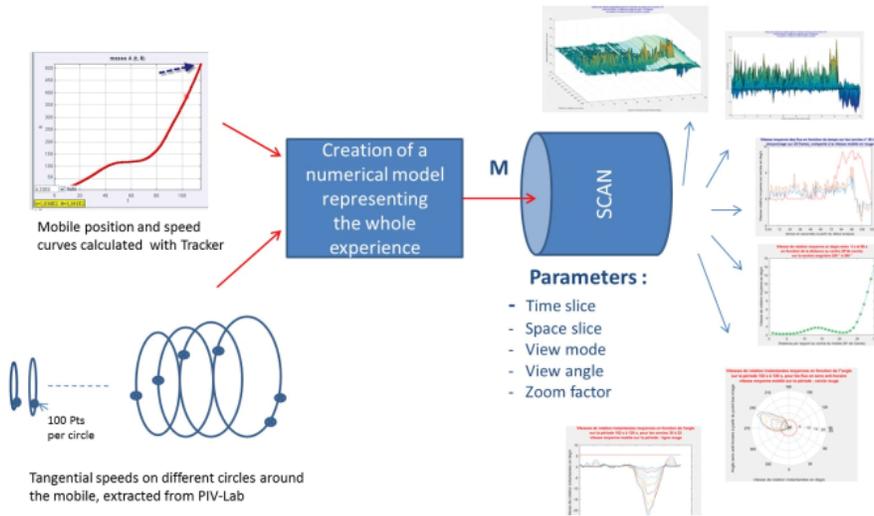
Figure M8. Scan-Flow-Mobile process.

process the air-flows speeds. In the software Tracker, one specific marker on the mobile is identified every second, so the software can compute the corresponding angular position and angular speed curve.

Then, a numerical model is built to synchronize all of these data as a function of time. Extraction of one minute of data at a frequency of 50 Hz represents nine million points. Once this model is in place, it is possible to choose different ways of representing and extracting the data: speed surface representation with time, mean circle speed representation, different levels of granularity, linear or polar views, etc. A zoom can be performed on a specific part of the data in a linear or polar way.

Experiments and Diagram Chosen for Results Presentation

These software procedures were used to perform a full analysis of the different experiments presented in the Results section. Each experiment has a report attached with the corresponding detailed results (internal reports at LAPDC that are identified by experiment number). We wanted to be sure that all factors capable of having an impact on the air flows and the mobile were taken into account. Sometimes, when looking at the results, we had to return to the original video in order to understand what had happened.

(Example: discovering that the introduction of smoke had an impact on the air-flow speed in a specific way.)

As described before, we conducted different types of experiments A, M, and PK from 2014 to 2016:

— A experiments using air flows as the driver of the mobile movement,
— M experiments using a motor (small electric engine),
— PK experiments where a person, with some supposed specific skills, was able to set the HM mobile in motion by placing their hand close, without touching it. (These experiments are not presented here as we are focusing on the methodological part.)

We will present the results of these experiments in the Results section, and we will compare them with each other. To do that, one diagram was extracted from each individual experience, which represents the mean air-flow speed close to the mobile (1.5–2 mm) compared with the mobile speed. The mean air-flow speed is evaluated as follows:

— On each experiment, an "impacted zone" is identified (the angular zone on the circles where the flow is focused). In some cases, there is no impacted zone and the complete circle is taken into account. This is done to avoid any side effects on the mean speed calculation that could lower the real air-flow speed
— On each concentric circle a mean value is calculated on the "impacted zone" at each time step, usually 20 ms
— So, for a specific circle, we have the curve as a function of time of this mean value (blue curve).
— We chose the circle which is at a distance of 1.5–2 mm from the HM mobile periphery in order to have a good idea of the air-flow speed close to the mobile (typically this is circle number 25, 26, or 27 depending on the experiment setup).

The mobile speed is obtained as described before (integration in the numerical model of the results obtained with the software Tracker).

Looking for Clear Anomalies versus Significant Deviations from the Null Hypothesis on a Set of Calibrated Experiences

For the use of this methodology to conduct a macro-PK test, as we defined in the Introduction (macro-PK or micro-PK), we do not need to use statistical tools to evaluate the rejection or not of the null hypothesis. In fact, we are looking for anomalous physical events inside the experiments. Contrary to a statistical approach, where experiments must be calibrated and repeated in the same design, using the same protocol, and in which all

data segments have to be considered in order to avoid an observer bias, here we are performing experiments and checking (in each case) if we can find some part where an anomalous physical (AP) event clearly appears.

This macro-AP is detected in our PK experiment if the ratio mobile speed / mobile periphery air-flow speed is significantly larger than one over the whole experiment or for a part of it. Indeed, as the other physical factors are already discarded (see Introduction), and this ratio being greater than 1 also discards the aerodynamics factor, then the macro-AP is detected. There is no need for statistics because this event alone is an anomalous perturbation (provided that a calculation of potential errors has been correctly done—see Discussion).

In the case that only a part of the experiment[4] is selected to bring to light this ratio above 1, it is necessary to show that the ratio reversal was not induced by a preceding event (for example, by a launching of the mobile at high speed by other means). Thanks to the PIV techniques used, it is easy for the outside observer to do this check, as any impact on the air flow or the mobile are recorded and can be followed and checked at a rate of 50 frames per second.

Results

A Experiments: HM Mobile Motion Driven by Generated Air Flows

To evaluate the ways to set the HM (described previously) in motion, three different experiments using air-flow generation (with pumps and/or fans) were set up. It is sometimes complex to set a mobile in motion in a steady fashion with a generated air flow in an open environment. The first task was to be able to start the motion of the mobile and evaluate what air-flow speed was required to achieve a mobile speed between 10 and 40 deg/s (typical speed reached with PKers). Therefore, the first two experiments used a mechanism with a pump aspirating a mix of smoke and air. The output of the pump was pushed inside a hose (small pipe such as the kind used in an aquarium), with one or several exits, bringing the air flow to the PIV bench (Figure R0). The third experiment was intended to study the minimum air-flow speed required to keep the mobile running, in a PK-like environment; it used a fan with separate input for the smoke introduction.

In the following sections, many images are used to describe the experiments and their results. These images mainly give a view from above, so the HM mobile appears as a disk.

Experiment A.1: Orthogonal air flow. The first experiment (#9628), performed in September 2015 on David Jamet's PIV bench, used the pump mechanism described above with a hose split for two exits, each one with
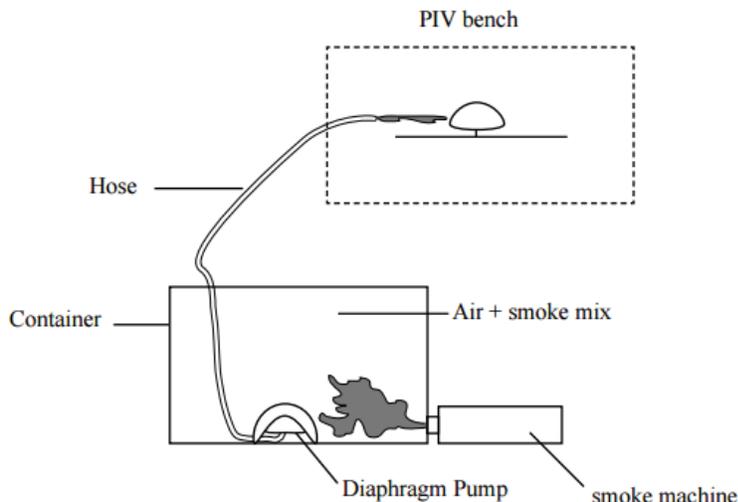
Figure R0. Mechanism for air-flow generation in A-1 and A-2 experiments.

a small tap. The first exit represented the main air flow, which we can see on the left of the HM, coming from the top of the figure (vertical flow on Figure R1). The second exit was horizontal and on the left, orthogonal to the preceding one (with the flow direction from left to right). Mobile motion has been produced with these two flows combined. The experiment duration was 120 s. After air-flow speed calculations using PIV LAB, the vector-field representation of the mean airflow speed around the mobile during these 120s is shown in Figure R2.

After Scan-Flow-Mobile processing, the evolution of the mean air-flow speed at 1.5 mm from the mobile (blue curve) compared to the mobile speed (red curve) during the 120 s duration is presented in Figure R3. The mobile began to move at about 65 s and reached a speed of 9.3 deg/s. To generate this motion, the mean tangential air-flow speed (converted to ro-tational speed) oscillated in the range 20–70 deg/s (with an approximate global mean of 40 deg/s).

Remarks: The global pump mechanism (smoke generation, pump, hose, and hose split) and the turbulence at the hose exits generated some speed oscillations that we can see on the graph (oscillation period in the range of 12–18 s). This experiment was insightful but not very efficient in the generation of motion. The mobile first oscillated around its axis without starting a circular motion. Then, after about 65 s, it began to move with a global flow which was a little stronger and better synchronized. In reality,
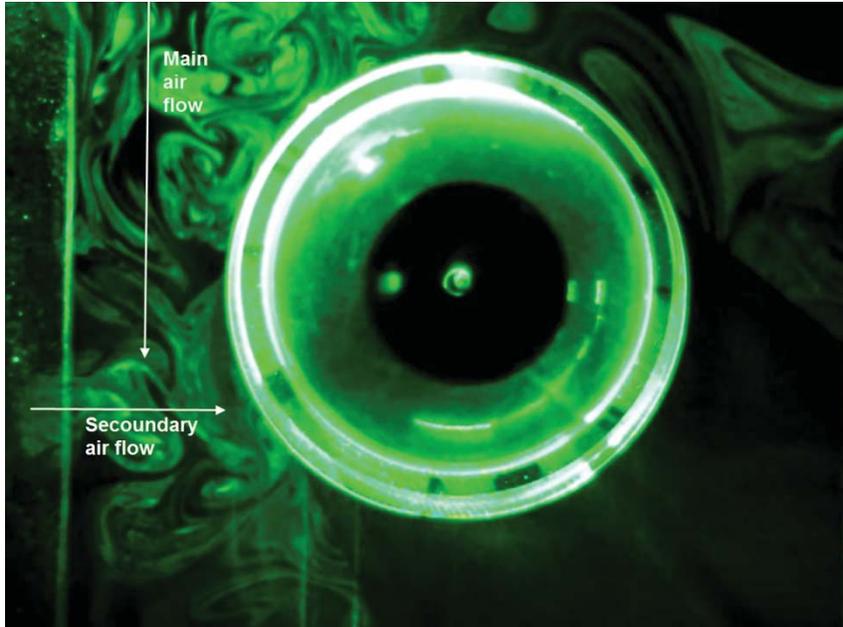
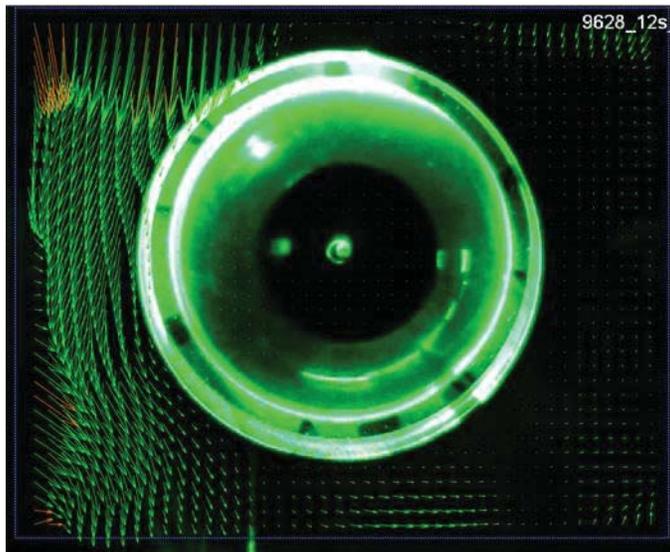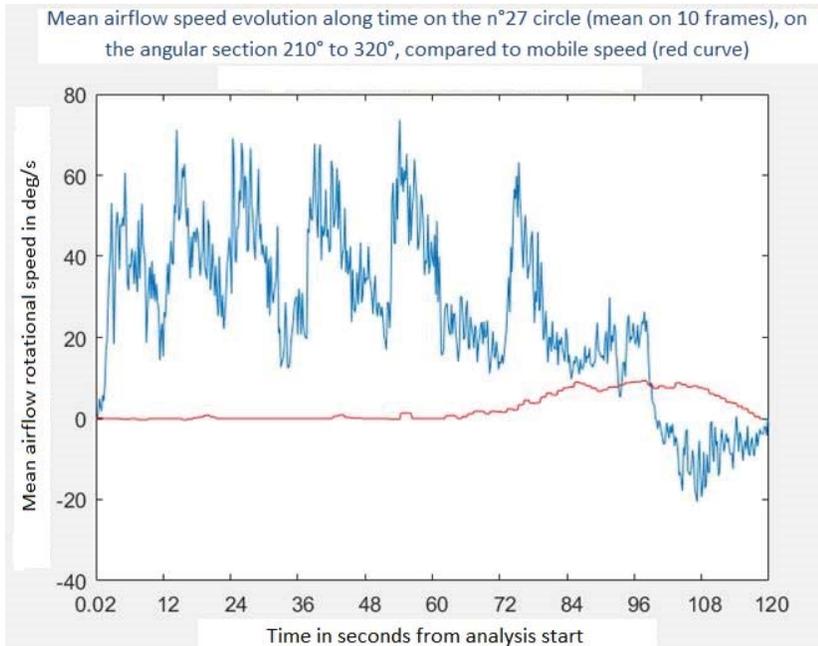**Figure R1. Combining vertical and horizontal air flows to set the HM in motion.**

Figure R2. Vector-field representation of the mean air flow speed around the mobile.

Mean airflow speed evolution along time on the n°27 circle (mean on 10 frames), on the angular section 210° to 320°, compared to mobile speed (red curve)

Figure R3. **Mean air flow speed close to the mobile compared with the mobile speed (red). The horizontal axis is the time elapsed and the vertical is the rotational speed in deg/s.**

the experience ended at 90 s, as the 10 deg/s mobile speed was reached. The portion of the graph after 90 s is not very meaningful: The first tap was closed allowing flow through the second exit, close to horizontal but slightly upward, which means that the air flow direction was reversed and the air-flow speed became negative. This explains the blue curve after 100 s.

Experiment A.2: Focused tangential air flow. To improve the efficiency of motion generation, a second experiment (#1251) was performed in February 2016 on the Davis Jamet PIV bench; only one focused tangential airflow was used (Figure R4). The recording duration was 84 s. Here again the focus was on starting the motion of the mobile. Unlike in experiment A.1, the hose is not split and is close to the mobile (light green part on the left of the image) which gives a more focused (air jet) air flow, which is very efficient at driving the mobile.

After the air-flow speed calculation with PIV LAB, Figure R5 shows the vector-field representation of the mean airflow speed around the mobile, during the 84 s of the experience.

After Scan-Flow-Mobile processing, Figure R6 shows the mean air-
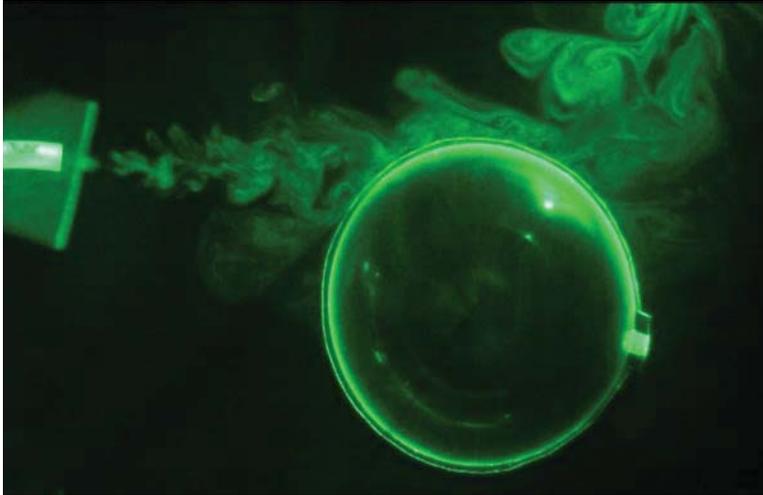
Figure R4. Focused tangential airflow to set the HM in motion.

flow speed evolution at a distance of 1.5 mm from the mobile (blue curve) compared with the mobile speed (red curve) over 84 s. The mobile started to move very quickly and reached a speed of 39.5 deg/s. To launch this motion, the mean tangential air-flow speed (converted to rotational speed) oscillated in the range 50–120 deg/s, with an approximate global mean of 75 deg/s during the launch period.

Remarks: The generation of motion was very efficient. A speed close to 40 deg/s was reached in just 50 s. As soon as the air flow had been stopped (56 s), the mobile took 25 s to return to being still (due to inertia and the action of air and needle friction).

Experiment A.3: Air flow generated by an axial fan with an artificial hand as the obstacle. The third experiment (#4327) took place on David Jamet's PIV bench in February 2017 (Dullin & Jamet 2017). One air flow was generated by an axial fan (not very focused), and a wood artificial hand was used to simulate the obstacle created by a hand in the air flow (Figure R7).

The idea behind this effort is to perform a type A experiment (mobile motion initiated by generated air flows) but with some PK experiment characteristics: a not very focused flow (axial fan) with a hand as an obstacle (a wood artificial hand). The mobile movement is induced, as in the Warcollier (1908) explanation, by the dissymmetry of forces around the HM; only one side is driven by the air flows while the other side is "protected" from the air
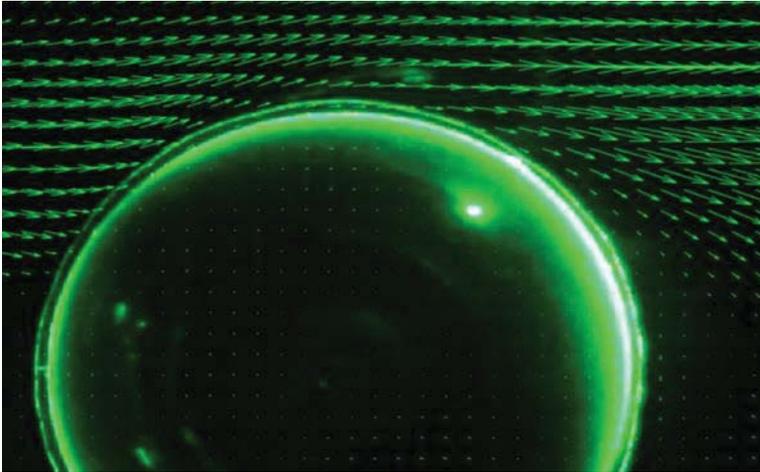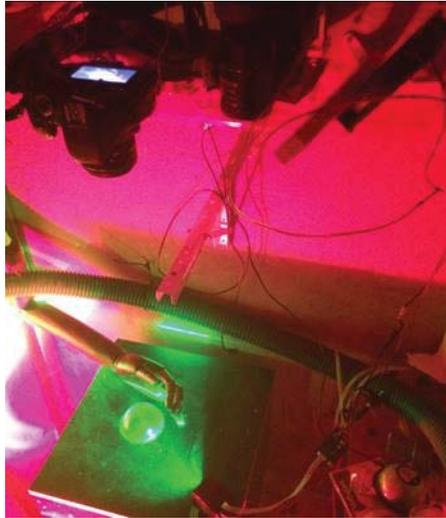
Figure R5. Vector-field representation of the mean air flow speed around the mobile.
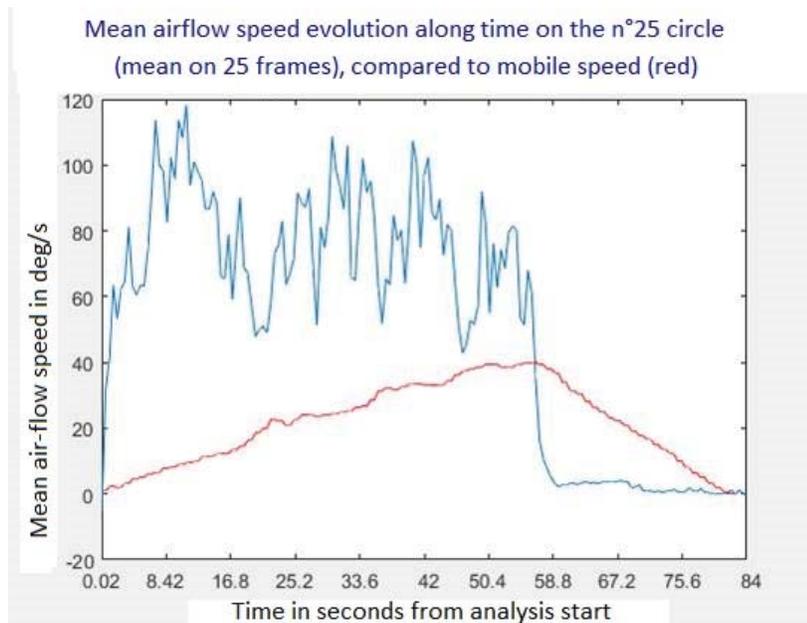
Figure R6. Mean air-flow speed close to the mobile compared with the mobile speed (red). The horizontal axis is the elapsed time, and the vertical axis is the rotational speed in deg/s.

Figure R7. Experimental setup with an artificial hand.

flows by the hand (Figure R8). The difference from the Warcollier experiment is that the air flows here are generated by an axial fan.

Working on the air-flow speeds, we tried to find the speed limit above which the mobile starts moving and maintains a steady rotation. An 18-s period of time when steady movement of the mobile was obtained was chosen. After air-flow speed calculations using PIV LAB and Scan-Flow-Mobile processing, Figure R10 shows the mean air-flow speed evolution 1.85 mm (blue curve) and 3.70 mm (orange curve) from the mobile compared with the mobile speed (red curve). The mobile speed was approximatively 4 deg/s. The mean tangential air-flow speed was 1.85 mm from the mobile oscillated from negative values (reverse flow during a few seconds around $t = 11$ s) to 100 deg/s with a global mean around 22 deg/s.

Remarks: As it is not generated using same mechanism as the other two A experiments, the same air-flow speed oscillations do not occur. The air flow here is much more evenly distributed (even if we can find a periodicity of about 2 s in the peaks). Several factors could explain this: the use of a fan, placed on the left of the image, rather than a focused air flow (so farther from the mobile) and the obstacles in the flow. The elementary peaks (every 2 s) in the air-flow speed do not impact the mobile speed because of its inertia. The air flow had a global impact on maintaining the mobile speed at an average value of 4 deg/s, which was the lowest speed that can be obtained with a steady movement. So, as expected, the efficiency was low: We achieved a speed of 4 deg/s for a mean speed of about 22 deg/s with some high speeds around 80–100 deg/s.
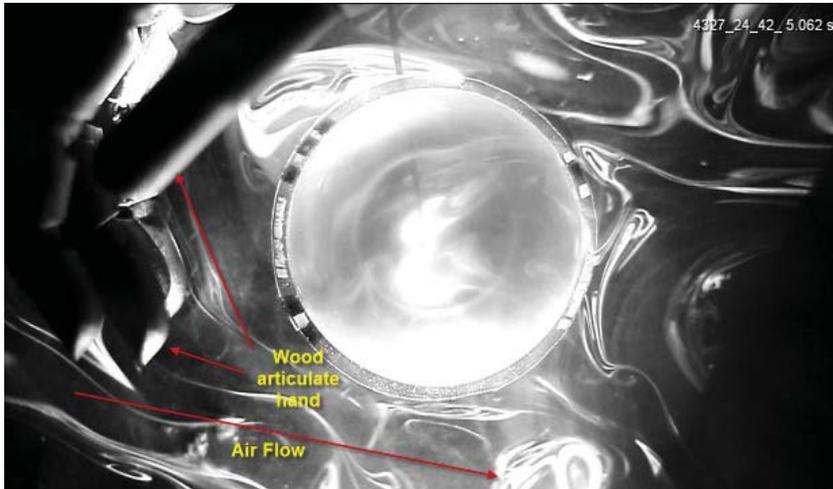
Figure R8. **Experimental setup with an artificial hand. Direction of the air flow, an artificial hand as an obstacle to a part of the airstream, leaving a tangential air flow on the other side of the mobile.**
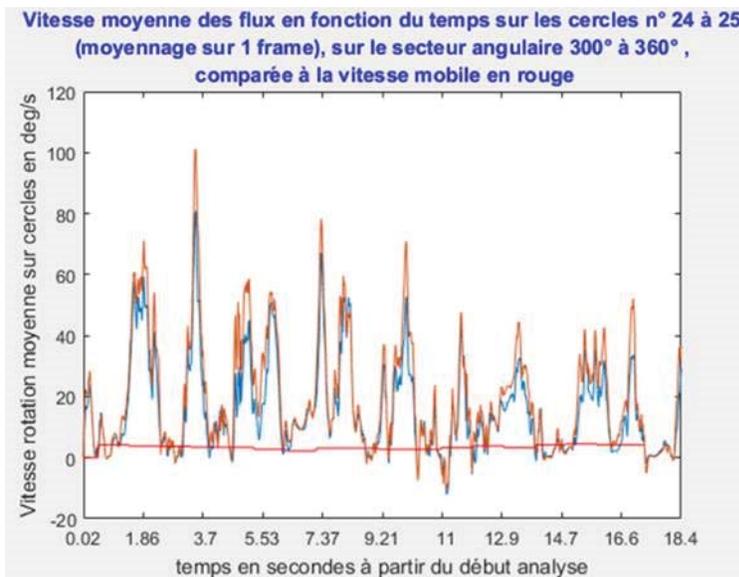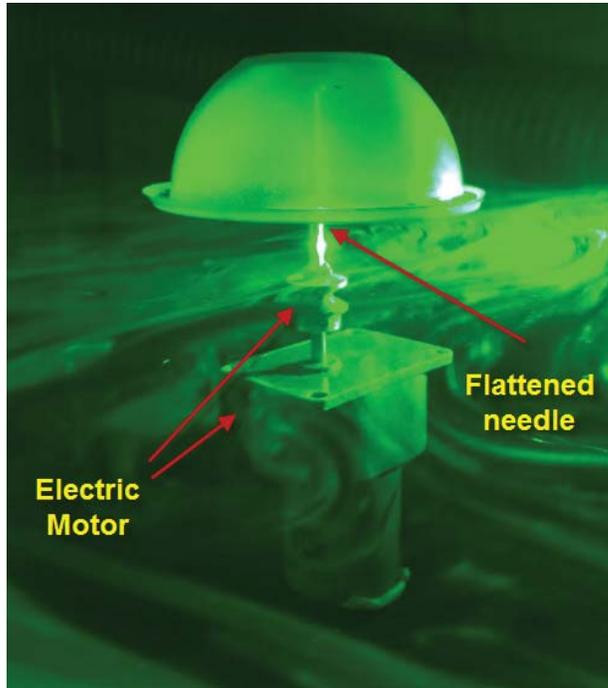

Figure R10. **Mean air-flow speeds close to the mobile compared with the mobile speed (red). The horizontal axis is the elapsed time, the vertical axis is the rotational speed in deg/s. Blue curve: air flows 1.85 mm from the mobile; orange curve: air flows 3.70 mm from the mobile.**

Figure R11. HM mobile attached to a needle spun by motor drive.

### *M Experiments: HM Motion Driven by a Motor*

In these two experiments, the HM mobile is driven into motion by a motor. In fact, the HM is placed on a needle (flattened a little on the top) with some "patafix" stuck on the mobile. This needle is then spun by a motor, so the spin drives the mobile, too (Figure R11).

Experiment M.1. This experiment (#2331) was performed in August 2016 on David Jamet's PIV bench. After air-flow speed calculations using PIV LAB and Scan-Flow-Mobile processing, Figure R12 shows the evolution of the mean air-flow speeds at the mobile periphery (and also at some farther distances from the mobile), compared with the mobile speed (red curve), over 52 s. The mobile driven by the spun needle achieved a speed of 25 deg/s and then 50 deg/s. The mean air-flow speed on circle 25, which is 1.8 mm from the mobile, was approximatively 5 deg/s. After the fast starting of the mobile motion, the air flows accelerated with a delay of between 0 and 7 s. It appears also that the air flows closer to the mobile were faster than those farther away. We can therefore conclude that the air flows were lightly driven by the mobile.
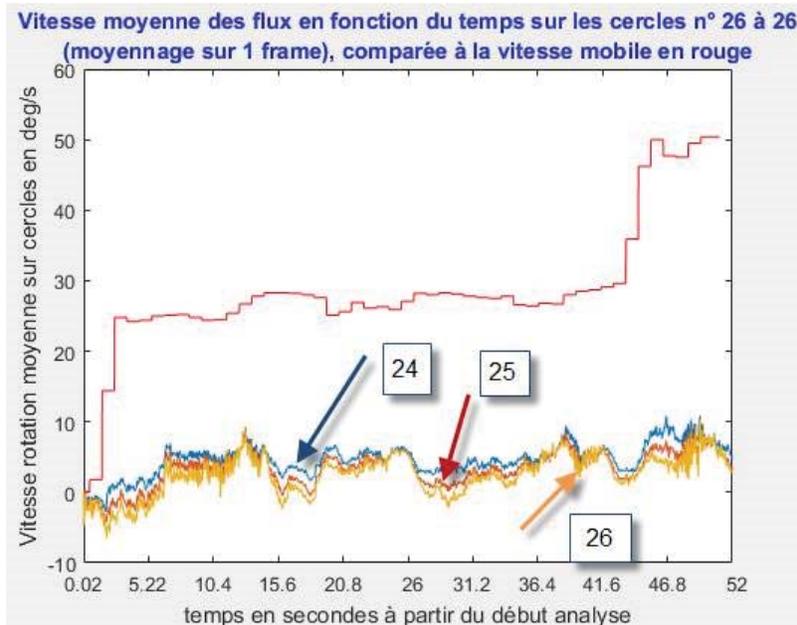
Figure R12. Mean air-flow speeds close to the mobile compared with the mobile speed (red). The horizontal axis is the elapsed time since the beginning; the vertical axis is the rotational speed in deg/s. Curve 24: mobile periphery; curve 25: 1.8 mm from the periphery; curve 26: 3.6 mm from periphery.

Experiment M.2: Motor-driven mobile with a large acceleration on the second part. This second experiment (#3039) was performed in November 2016 on David Jamet's PIV bench. It was done to confirm the first experiment and also to further study the air-flow behavior in the case of strong acceleration of the mobile. After air-flow speed calculations using PIV LAB and Scan-Flow-Mobile processing, the evolution of the mean air-flow speeds 1.8 mm (curve 24) and 10.6 mm (curve 30) from the mobile compared with the mobile speed (red curve) over 63 s is shown in Figure R13. The mobile, driven by the spun needle, reached a speed of 17 deg/s, then stopped at $t = 42$ s. Then, with a very strong acceleration, it quickly spun up to 70 deg/s. Accordingly, the mean air-flow was initially around 5 deg/s and it then increased to 22 deg/s. Air entrainment by the mobile is clearly visible here: The air-flow speed closer to the mobile periphery (circle 24) is higher than farther out (circle 30). When mobile acceleration occurred, air-flow speeds became greater also.
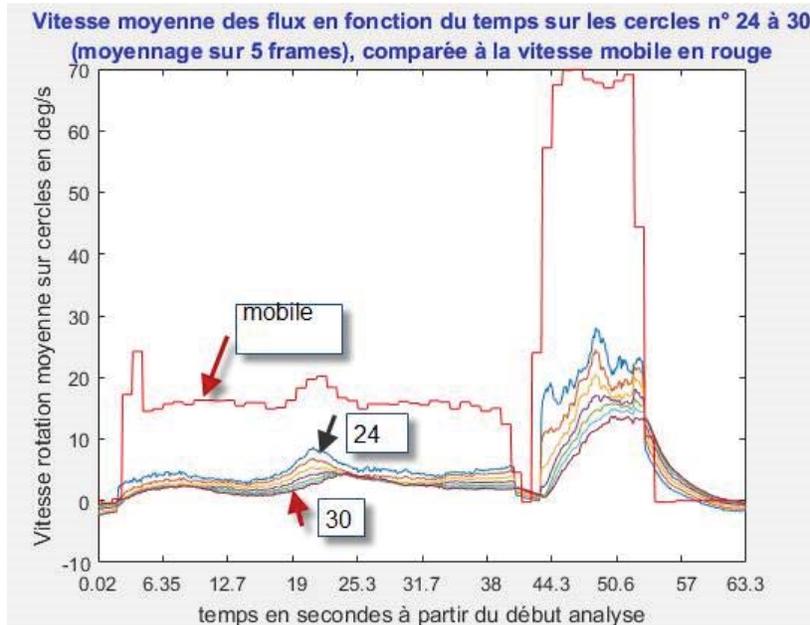
**Figure R13. Mean air-flow speeds at different distances from the mobile com-
pared with the mobile speed (red). The horizontal axis is the time
elapsed since the beginning, the vertical axis is the rotational
speed in deg/s. Curve 24: at 1.8 mm from the mobile periphery;
curve 30: at 10.6 mm from periphery; other curves: between.**

Figure R14 shows the air-flow speed vector field, calculated between
two images, during the period of strong acceleration. The mobile is driven
in a clockwise direction and drives the air-flows (green arrows). However,
it is important to notice that the mean air-flow speed remained much lower
than the mobile speed, as in the M1 experiment. In the comparison part, this
experiment will be divided into two parts: "low speed" from 0 to 42 s and
"high speed" from 42 to 63 s.

Comparison between Results of A and of M Experiments

To compare the preceding experiments, we chose in the Methods section
to evaluate the ratio: mobile speed / mobile periphery air-flow speed. We
took as periphery air-flow speed the one situated at least 1.5 mm (A1 and
A2 experiments) from the mobile periphery, to avoid potential calculation
errors (see Discussion: DPIV algorithm, where DPIV is digital PIV). Six
results are presented in the table below comparing mean mobile periphery
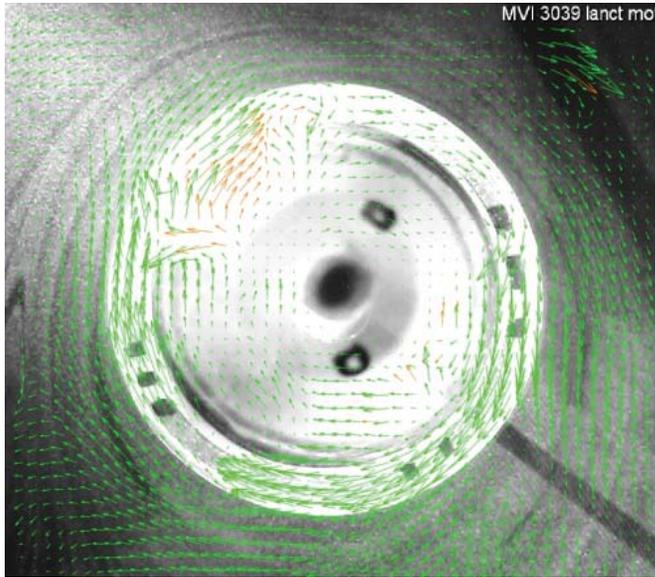
**Figure R14. PIV results: speed vectors field between two sequential images
                separated by 48.735 s.**

air-flow speed (named "Air-flow speed"), mean mobile speed (named "Mo-
bile speed"), and the ratio between the two (Table 1).

The 6 results are placed on the diagram in Figure R27. The different ex-
periments are placed on the horizontal axis in the order used to present them
above. They are grouped by category (A, M). The vertical axis represents
the ratio value.

The diagram shows a clear separation between air-flow experiments
(A), for which the ratio is lower than 1 (max 0.53), and the motor-driven
category (M), for which the ratio is above 1 (min 2.92). These consistent
results across different experiments contribute to the validation of the mea-
surement protocol.

Conclusion

The methodology proposed here provides a way to identify if the aerody-
namic effects can be or not be the only cause of the spinning of a light ob-
ject in a non-confined environment. In the experiments presented, and the
Figure R27 outline of the M category of experiments, aerodynamic effects
could not explain the mobile spinning (which is correct as the movement is
due to the torque of the electric motor on the needle).

TABLE 1
Results Comparison between the Two Categories of Experiment

	A 1	A2	A3	M1	M2a	M2b
Air-flow speed	40	75	22	5	5	24
Mobile speed	9.3	39.5	4	28	17	70
Ratio	0.23	0.53	0.18	5.60	3.40	2.92

The methods developed provide many tools with which to study in more detail what is really happening to the air flows and the spinning object during the experience. Also, the techniques proposed can easily detect any trickery involving aerodynamic forces used to move the mobile (such as mouth air blowing or hand movements).

This approach could be a good candidate to evaluate macro-PK tests in a non-confined environment. As this set of experiments constitutes a pilot study (the first time this kind of technology is used on this topic), the technology and the protocols used need to be confirmed and improved by other experiments in order to confirm the results obtained. We are looking to improve the total measurement process documentation, so that other laboratories can test it in their experiments.
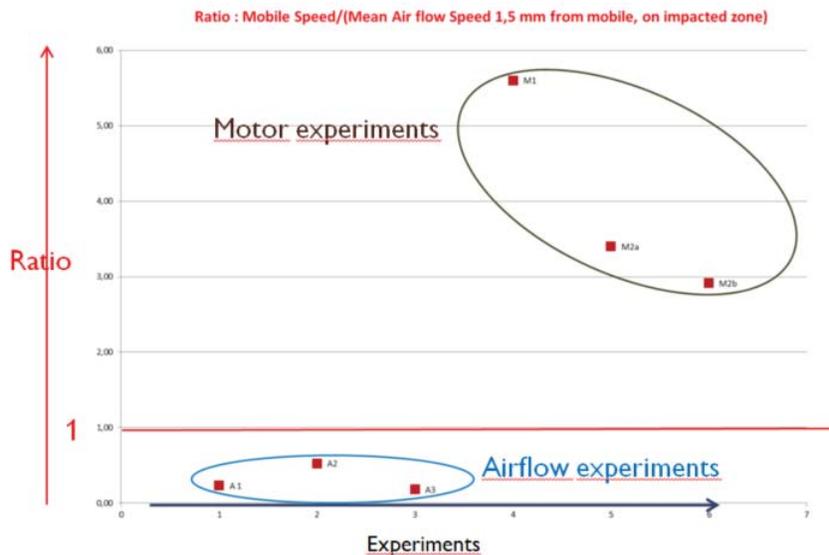
Figure R27. Results comparison between two categories of experiment.

Discussion

Plan Approach versus 3D Approach

One could argue that the slice chosen to make the laser plan might not be representative of the air flows around the mobile on other slices. To answer this point, we can say that:

— We are not in a turbulent mode (speeds are low), so air flows are homogeneous around the mobile. There is no shear fracture in the flow vertically. If this was the case, we could detect it with a thorough analysis of the PIV results in the plan (many patterns would disappear from one image to the next).

— A experiments are processed in the same way as those performed using PKers, and we need to have the air-flow driving force in the same plan as the laser to be able to analyze it.

Furthermore, in our current research, we also have conducted some experiments with vertical PIV (to investigate the vertical air flows). These experiments have given no indication of flaws in the method described in this paper.

Tolerance on Ratio Evaluation

To compute the possible error in the ratio evaluation that we present in the Results section, we must look at possible sources of error:

The uncertainty parameters associated with the air-flow speed calculations such as:

- the difference between fluid and particle velocity,
- image acquisition error and frequency acquisition tolerance,
- calibration,
- the DPIV algorithm (image treatment),
- impacted zone and circle mean speed determination,
- mean choice to be used in the ratio for the global experience.

The uncertainty parameters associated with the HM mobile speed calculation such as:

- mobile image acquisition error (same as for the air flow),
- marker angular position measured by the software Tracker,
- mean choice to be used in the ratio for the global experience.

We will now look at some of these parameters.

Difference between Fluid and Particle Velocity

In a continuously accelerating element of fluid, the velocity lag U_s, between particle velocity U_p, and fluid velocity U, can be written using Stokes' drag law, as in Figure D1 (Raffel et al. 2007), where d_p is the particle diameter, ρ_p is the particle density, ρ is the fluid density, μ is the fluid dynamic viscosity, and a is acceleration.

$$U_s = U_p - U = d_p^2 \frac{\rho_p - \rho}{18\mu} a$$

Figure D1. Stokes' drag law.

The size of the elementary smoke patterns followed by PIV LAB in our experiment are estimated to be in the range of 1–8 pixels. So, in the worst-case scenario, we have 4 pixels as d_p. In most of our calibrations, 1 pixel corresponds to 0.18 mm, so $d_p = 0.72$ mm. Smoke particles are made of glycol which has a density of 1.110 kg/m³. Using the parameters for air at 20 °C, we obtain $U_s = 0.4a$. The mean air-flow acceleration in the A experiment is close to zero, sometimes even negative (the only changes in speed are due to oscillations around the same value because of the experiment setup) (Dullin 2015–2017). Therefore, this parameter has no effect.

At the beginning of the M1 experiment, the air flow increases from 0 to 8 deg/s in 7 seconds, so the acceleration is 1.14 (deg/s)/s. That gives a speed error of 0.4 * 1.14 = 0.46 deg/s (the speed of the air increases by 0.46 deg/s).

In the second part of the M2 experiment, the speed increases from 0 to 20 deg/s in one second (blue curve). So, $a = 20$ (deg/s)/s implies $U_s = 0.4 *$ $20 = 8$ deg/s, and the air-flow speed could be 28 deg/s instead of 20 deg/s. We can easily correlate this with the next part of the curve, which effectively peaks at 28 deg/s, as the smoke particles are now moving at almost the same speed as the air because the acceleration has returned to zero.

In the T experiment, only the T.1 part shows acceleration of the air flow (small), with the mean speed changing from 2.5 to 5 deg/s between 50 s and 75 s; this means that acceleration is 0.1 (deg/s)/s. So, the speed error is 0.4 * 0.1 = 0.04 deg/s, which is marginal compared with the other error factors.

In conclusion, this factor has no real impact on the results seen above. It increases the ratio for the second part of the M.2 experiment from 0.34 to 0.37 because of the very large acceleration of the motor drive.

Image Acquisition Error and Frequency Acquisition Tolerance

A continuous wave laser is used in the experiments, alongside a good quality camera (CANON 600 D with a resolution of 1080 * 720 pixels. All

experiments capture images at a rate of 50 image/s. Error at this level is marginal compared with the other error sources.

Calibration

The same type of mobile is used for all experiments. Its diameter (85 mm) is used in the PIV LAB calibration (Figure D2). So, the uncertainty in its value is associated with the drawing used to define the diameter on the image. We can estimate this at 2 pixels on each side, giving 0.18 * 4 = 0. 72 mm or 0.72/85 = 0.8%.

DPIV Algorithm (Image Treatment)

This is an extract from Thielicke's thesis (Thielicke 2014):

> In DPIV, the particle displacement is calculated for groups of particles by evaluating the cross-correlation of many small subimages (interrogation areas). The correlation yields the most probable displacement for a group of particles traveling in a straight line between image A and image B. Under optimal conditions, the bias error of the window deformation DPIV algorithms used is smaller than 0.005 pixels and the random error is below 0.02 pixels. When the average displacement in a DPIV study is around 6 pixels, the displacement error goes below 0.42%.
>
> In our case (small speeds), the average speed in an A experiment is around 40 mm/s (75 mm/s maximum in A2), which gives an average displacement of 4 pixels (8 pixels maximum) for a 50-Hz image capture frequency and a pixel size of 0.18 mm. With M and T experiments, the average speed is more like 10 mm/s, which gives an average displacement of 1 pixel for the same image capture rate. So, we can assume an error of 1% for this part of the process.
>
> It is important to note that very close to the front of the object (closer than 1 mm), DPIV gives a decreased air-flow speed if the mobile is slower and an increased air-flow speed if the mobile is faster. However:
>
> The speed values are taken at least 1.5 mm from the mobile.
>
> If some error were due to this factor, our results are reinforced because the air-flow speed for A experiments should be increased (air flow faster than the mobile) and the air-flow speed for T experiments should be decreased (air flow slower than the mobile).

Further studies are required to evaluate the impact of the window interrogation choice (Thielicke & Stamhuis 2014) on the high air-flow speed treatment (for A experiments). In fact, the speed values in A experiments could be higher than our current evaluation (which would further reinforce our results). Work has already been done on the A2 experiment with the higher air-flow speed input.
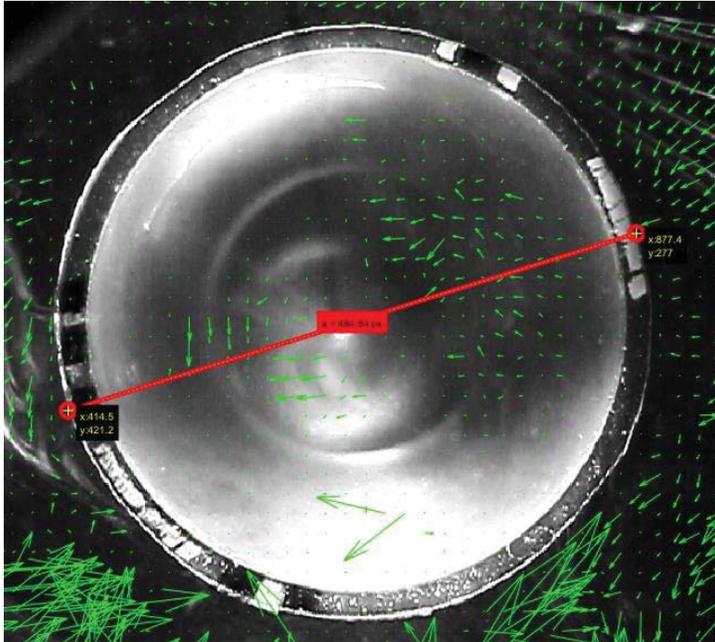
Figure D2. Calibration in PIV LAB using HM mobile diameter (85 mm).

Impacted Zone and Circle Mean Speed Determination

There is uncertainty in the exact impacted zone chosen when computing the mean speed on the circle (start angle, end angle) at each time step; the estimated error is ±2%.

When we evaluate the mean speed to be taken into account for the air flow from the preceding curves, even if we also use a software calculation to confirm it, there is some uncertainty depending on the part of the curve taken into account. Some other operator could have chosen a slightly different value. We estimate the error to be ±3%.

So we have a combined error risk of ±5% which gives a 10% potential error in the air-flow speed.

Marker Angular Position Measured in Tracker and Mobile Speed Evaluation

Using the software Tracker, we pinpoint the marker position at each second of the experiment. The software deduces the cumulative mobile angular position and its angular speed at each time stamp. When we locate the marker

position, there could be a ±1-degree error in the angular position, although this is not cumulative, as we redefine the exact position of the marker each second. So, between two points there could be a 2-degree error in the measurement which impacts the speed calculation between these points. However, at the next point this error will be corrected in the other direction because we always process a new measurement for each step. We conclude that the main error happens when we evaluate the mean of the global curve in order to calculate the ratio. We have estimated this risk to be the same as for the air flow (±3%), implying a global risk of 6%.

Conclusion: Error Estimation on the Ratio

To calculate the uncertainty on the mean air-flow speed, we add the following individual errors:

— 0.8% for the calibration,
— 1% for the DPIV treatment,
— 10% for the mean calculation,

which gives a total error of 11.8%. For the mean mobile speed, we calculated an error of 6%. Finally, we have an uncertainty of 11.8 + 6 = 17.8% (±8.9%) in the value of the ratio.

Consequences of the Ratio Diagram

The highest ratio in the A experiment (A2) is 0.53; 8.9% above this point gives 0.58. The lowest ratio in the M experiment has a value of 2.92; 8.9% below this point gives 2.68. Therefore, we have a ratio of 5 between the two closest points of the A and M categories. The uncertainty error in the ratio cannot explain the differences between these two categories (driven by air flows and motor-driven).

Acknowledgments

Notes

¹ TK: At the LAPDC we use TK for telekinesis. For this paper, we will use PK for psychokinesis. This point is discussed at the end of the Introduction.

² As an example, here is a search on Youtube with the *psychokinesis* keyword: https://www.youtube.com/results?search_query=psychokinesis

³ As an example, here is a search for psi wheels:
http://www.internationalskeptics.com/forums/showthread.php?t=117190&highlight=psi+wheel

⁴ Sections of the experiment are also chosen according to measurement conditions (for example, a video showing good lighting and good smoke-particle seeding).

⁵ AFVL: Association Francophone de Vélocimétrie Laser (Laser Velocimetry French-speaking Association).

⁶ IMI: Institut Métapsychique International.

References Cited

Alvarado, C. (2006). Human radiations: Concepts of force in mesmerism, spiritualism, and psychical research. *Journal of the Society for Psychical Research, 70.3*:138–162.

Archat, P. (1908). Recherche expérimentale de l'action motrice sans contact. *Annales des Sciences Psychiques (section Actes de la Société Universelle d'Ëtudes Psychiques), 17–18*(16 June to 1 July):198–201.

Auerbach, L. (1996). *Mind over Matter*. Kensington.

Dullin, E. (2015–2017). Experiment setting and report analysis (9628, 1251, 4327, 2331, 3039, 81L-Part 2, 7076 start, 7076 launched, 2756). *LAPDC Internal Reports.*

Dullin, E., & Jamet, D. (2017). Du moteur à fluide à la PK sur le net (From the bioforce motor to the PK on the Internet). *Métapsychique*, 1:76–85.

Egely Wheel (2017). http://egelywheel.net/

Evrard, R. (2016). *Enquête sur 150 ans de parapsychologie.* Editions Trajectoire.

Giuditta, A. (2014). On the human bioenergy field. *WISE Journal, 3*(3).

Hofmann, A. (1919/1992). *Das Rätsel der Handstrahlen: Eine Experimental Studie*. Leipzig: Oswald Mutze.

Hansen, J. N., & Lieberman, J. A. (2013). Use of a torsion pendulum balance to detect and characterize what may be a human bioenergy field. *Journal of Scientific Exploration, 27*(2):199–219.

Jahn, R. G., & Dunne, B. J. (2011). *Consciousness and the Source of Reality—The PEAR Odyssey.* Princeton, NJ: ICRL Press.

Krmessky, J. (1975). Psychokinesis Research in Czech–Soviet and Czech parapsychology research. U.S. Defense Intelligence Agency, declassified, p. 47.

Kruth, J. G. (2016). Experimental PK Studies with Exceptional Participants—Rhine Research Center. *Parapsychological Association Convention* poster.

Martin, C. (1926). Essais expérimentaux sur les effets moteurs du supposé fluide magnétique humain. *Revue Métapsychique, 2*:125.

May, E. C., Utts, J. M., & Spottiswoode, S. J. P. (1995). Decision Augmentation Theory: Toward a model of anomalous phenomena. *The Journal of Parapsychology, 59*(September):195–220.

Perelman, Y. (1913). *Physics for Entertainment* [in Russian]. [Reference is made to a communication

to the Moscow Medical Society from N. P. Nechayev in 1876, entitled "The Gyration of Light Bodies Caused by the Heat of the Hand."]

Raffel, M., Willert, C., Wereley, S., & Kompenhans, J. (2007). *Particle Image Velocimetry (2nd Edition).* Springer Publishing,

Rudkin, J. (2001). The Egely Wheel—A Telekinesis detector? *Society for Psychical Research Paranormal Review, 19*(July).

Stine, G. H. (1985). *On the Frontiers of Science—Strange Machines You Can Build.* Collier Macmillan.

Thielicke, W. (2014). The Flapping Flight of Birds—Analysis and Application. Ph.D. Thesis, Rijksuniversiteit Groningen. http://irs.ub.rug.nl/ppn/382783069

Thielicke, W., & Stamhuis, E. J. (2014). PIV LAB: Time-Resolved Digital Particle Image Velocimetry Tool for MATLAB. https://figshare.com/articles/PIVlab_version_1_35/1092508

Tromelin, Comte de, G. (1907). *Les Mystères de l'Univers*—Collection Bon. Paris: Bibliothèque Universelle Beaudelot.

Tromelin, Comte de, G. (1912). Le fluide vital ou force biolique chez l'humain normal. *Le Monde Psychique-Juillet 1912 de l'institut de Recherches Psychiques de France:*432–439.

Varvoglis, M., & Bancel, P. (2015). Micro-Psychokinesis. In *Parapsychology: A Handbook for the 21st Century,* Chapter 20, edited by Etzel Cardeña, John Palmer, and David Marcusson-Clavertz, Jefferson, NC: McFarland.

Warcollier, M. (1908). Le "Moteur à fluide" du comte de Tromelin. *Annales des Sciences Psychiques, 1908*:201–203.

Watkins, G. (2015). Macro-Psychokinesis. In *Parapsychology: A Handbook for the 21st Century,* Chapter 6, edited by Etzel Cardeña, John Palmer, and David Marcusson-Clavertz, Jefferson, NC: McFarland.